THE JOURNAL OF PHYSICAL CHEMISTRY Letters

Letter

pubs.acs.org/JPCL

Reversible Adsorption of Outer-Sphere Redox Molecules at Pt Electrodes

Dileep Mampallil, Klaus Mathwig, Shuo Kang, and Serge G. Lemay*

MESA+ Institute for Nanotechnology, University of Twente, Carre 4409, Achterhorst, 7500AE Enschede, The Netherlands

Supporting Information

ABSTRACT: Adsorption often dominates the response of nanofluidic systems due to their high surface-to-volume ratios. Here we harness this sensitivity to investigate the reversible adsorption of outer-sphere redox species at electrodes, a phenomenon that is easily overlooked in bulk measurements. We find that even though adsorption does not necessarily play a role in the electron-transfer process, such adsorption is nevertheless ubiquitous for the widely used outer-sphere species. We investigate the physical factors driving adsorption and find that this counterintuitive behavior is mediated by the anionic species in the supporting electrolyte, closely following the well-known Hofmeister series. Our results provide foundations both for theoretical studies of the underlying mechanisms and for contriving strategies to control adsorption in micro/nanoscale electrochemical transducers where surface effects are dominant.

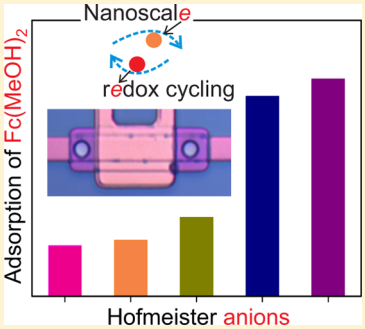

SECTION: Liquids; Chemical and Dynamical Processes in Solution

An ideal outer-sphere electron-transfer reaction between a molecule in solution and an electrode involves the tunnelling of one or more electrons without significant chemical interactions developing between the two. This is in contrast with inner-sphere reactions that by definition entail some form of linkage between the molecule and the surface – ranging from covalent binding to adsorption at specific sites – before the reaction can proceed.[1] Outer-sphere reactions are often associated with fast electron transfer that is relatively independent of the nature of the substrate.

Classification into inner- and outer-sphere reactions, however, pertains only to the electron-transfer mechanism. A reaction proceeding along an outer-sphere pathway does not in itself rule out the possibility of residual interactions between the electrode and the molecule(s) involved, insofar as such interactions do not influence the electron-transfer process. A prototypical illustration is the case of a redox species immobilized at an electrode, an approach that was famously employed to quantitatively study electron tunnelling in outer-sphere reactions.[2] One can similarly envision that residual interactions between the reduced or oxidized forms of a redox species and an electrode lead to some degree of weak adsorption. While not directly involved in electron transfer, such adsorption can nonetheless affect electrochemical experiments by influencing mass transport.

It is widely accepted that small cations and anions in solution can adsorb onto solid electrodes.[3] In general terms, adsorption of a particular species results from a difference in (Gibbs) free energy between the species in bulk solution and at the surface. The microscopic driving mechanism can be enthalpic, entropic, or some combination thereof, and the degree of adsorption is thus sensitive to a broad range of tunable parameters that include temperature, the nature of the solvent, the degree of electrification of the electrode, the presence of other species at the surface and, of course, the identity of the adsorbing species. For example, the degree of specific adsorption of anions on metal electrodes is ion-specific and increases in the order F^-, SO_4^{2-}, Cl^-, Br^-, I^-.[4−6] Specific adsorption of ions can in turn change an electrode's interfacial potential distribution[7,8] and potential of zero charge,[9,10] with the largest shift arising for the most polarizable ions (e.g., Br^- and I^-). It has further been argued that specific adsorption of anions can influence electrochemical processes, for example, through the formation of "bridges" between a redox-active species and an electrode that increase the reaction rate.[8,11]

Given the ubiquity of adsorption, it is reasonable to expect that redox species can also exhibit some level of adsorption at electrodes, even when this is not a necessary step in the electron-transfer process. Here we use the term adsorption in its broadest sense to refer to a total surface excess that includes both physi- and chemisorption. Measuring such adsorption, however, represents a significant challenge because the corresponding surface concentration can correspond to only a small fraction of a monolayer. For example, quartz microbalance experiments were initially interpreted as indicating detectable levels of adsorption, but this interpretation was later disputed when it was suggested that the data could be understood solely by invoking relatively subtle changes in solution density and viscosity caused by redox reactions.[12] Less controversially, metal nanoparticles functionalized with ferrocene groups were also found to exhibit adsorption at Pt electrodes.[13]

Received: November 28, 2013
Accepted: January 27, 2014
Published: January 27, 2014

One situation in which even a mild degree of adsorption can have a significant impact on measurements is in micro- or nanofluidic measurement systems. The past decade has seen a surge of activity aimed at creating miniaturized channels and electrodes suitable for electrochemical measurements on minute amounts of solution.[14] The motivations for these advances range from fundamental studies of electron transfer and mass transport to the development of miniaturized analytical methods suitable for point-of-care diagnostics.[15] An inherent feature of such miniaturized systems is their high surface-to-volume ratio,[16] which can greatly magnify the influence of any surface interaction compared with measurements at more conventional macroscopic or micrometer-scale electrodes. Over recent years, our group has performed a series of redox-cycling measurements at pairs of electrodes separated by nanogaps with heights below 100 nm, suggesting that reversible adsorption is ubiquitous in these systems. We find that at high concentrations of redox species adsorption dominates the noise properties of nanoscale sensors[18,19] and limits their response time,[20] while at ultralow concentrations it significantly decreases the current levels generated by individual molecules.[21,22] Quantitatively understanding electrochemical processes in these systems thus requires revisiting the possible influence of adsorption.

Here we take advantage of our nanofluidic approach to investigate adsorption of outer-sphere redox couples. The nanogap geometry facilitates the measurements in three distinct manners: (1) it creates a very high surface-to-volume ratio, which increases the relative number of adsorbed molecules and therefore magnifies the influence of adsorption at the surfaces, (2) it ensures that the absolute number of redox molecules in the detection region remains relatively small, which allows stochastic spectroscopy methods to be applied to the signals, and (3) it permits very efficient redox cycling, such that minute amounts of analyte, even down to single molecules at subnanomolar concentrations, can be detected.[21,22] These factors render the method extremely sensitive even to small amount of adsorption. Our observations provide a solid basis for understanding the underlying physical mechanisms responsible for the adsorption.

A sketch of a nanogap device is shown in Figure 1a. A detailed method for making the devices using optical lithography is given in the Supporting Information (SI), and an optical image of a completed device is shown in Figure 1b. All data shown here employ Pt electrodes based on thin films created by electron-beam evaporation. The active volume, namely, the volume sandwiched between the two redox-cycling electrodes, is defined by the length of the top electrode, L_a, the width of the bottom electrode, w_b, and the separation between the electrodes, h. Here we employ two distinct families of devices, types 1 and 2, with $L_a \times w_b \times h$ = 100 μm × 3 μm × 130 nm and 10 μm × 3 μm × 60 nm, respectively. The redox-cycling current in a device is given by $i_{lim} = (enD/h^2)N_{sol}$, where $-e$ is the charge of the electron, n is the number of electrons transferred per cycle, D is the diffusion coefficient, and N_{sol} is the number of molecules in solution inside the active volume at a given instant. On average, $\langle N_{sol}\rangle = N_A L_a w_b h c$, where N_A is Avogadro's number and c is the molar concentration of the redox species in the reservoir of the device, which is independent of the level of adsorption at the surface of the electrodes.

We first illustrate how reversible adsorption can be directly observed in nanofluidic systems through two separate experiments, potential-step amperometry and electrochemical correlation spectroscopy, as summarized in Figure 2. Each of these experiments furnishes two independent signatures of adsorption, emphasizing its broad impact on redox-cycling measurements.

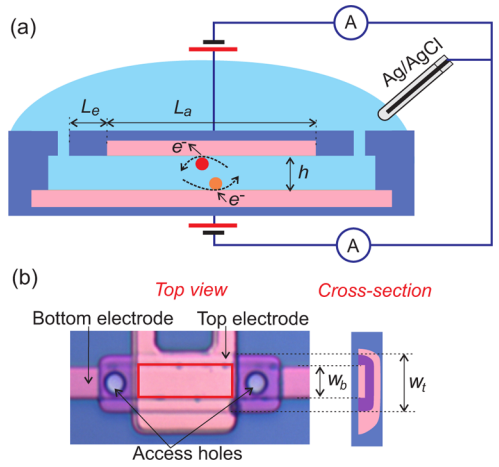

Figure 1. (a) Schematic diagram of the longitudinal cross-section of a nanogap device used for redox cycling. The two electrodes are shown in pink. Also identified are the height of the nanochannel, h, the length of the active redox-cycling region, L_a, and the length of the access channels, L_e. (b) Top-view optical image of a device and schematic illustration of its cross-section. The active region (red rectangle) is defined as the volume between the top and the bottom electrodes. The widths of the bottom electrode and of the nanochannel are w_b and w_t, respectively.

Potential-step amperometry gives the clearest qualitative signature of adsorption in nanogap devices by exploiting the fact that the degree of adsorption typically depends on the electrode potential. For example, adsorption of the oxidized form of ferrocene is observed to be enhanced with increasing electrode potential.[18,20] Abruptly stepping the potential of an electrode to a higher potential therefore causes a temporary decrease in the analyte concentration inside the nanogap as more molecules become bound to the electrode; this local depletion then recovers over time as more molecules diffuse from a large reservoir outside the device. Correspondingly, the redox cycling current, which is proportional to the local concentration of freely diffusing analyte inside the nanodevice, is suppressed immediately following the potential step. It then gradually recovers over time, the rate of recovery being dictated by diffusion from the external reservoir and into the nanodevice. Because this diffusion is hindered by adsorption, slower recovery indicates increased adsorption. Both the magnitude of the initial current suppression and the duration of the recovery are thus indications of the degree of adsorption.[20]

This phenomenon is illustrated in Figure 2a for 1 mM $Fc(MeOH)_2$ in 1 M KCl supporting electrolyte for a range of temperatures in device type 1. The bottom electrode (reducing) was kept at 0 V. At room temperature (22 °C), a ∼50% suppression of the limiting current is observed upon stepping the potential of the top electrode (oxidizing) from 0 to 0.4 V, indicating enhanced adsorption at the oxidizing electrode. The current then recovers to its diffusion-limited value after ∼20 s. As the temperature is increased, the amplitude of the departure from the limiting current and duration of the transient both decrease, reaching <5% and 5 s,

dx.doi.org/10.1021/jz402592n | J. Phys. Chem. Lett. 2014, 5, 636−640

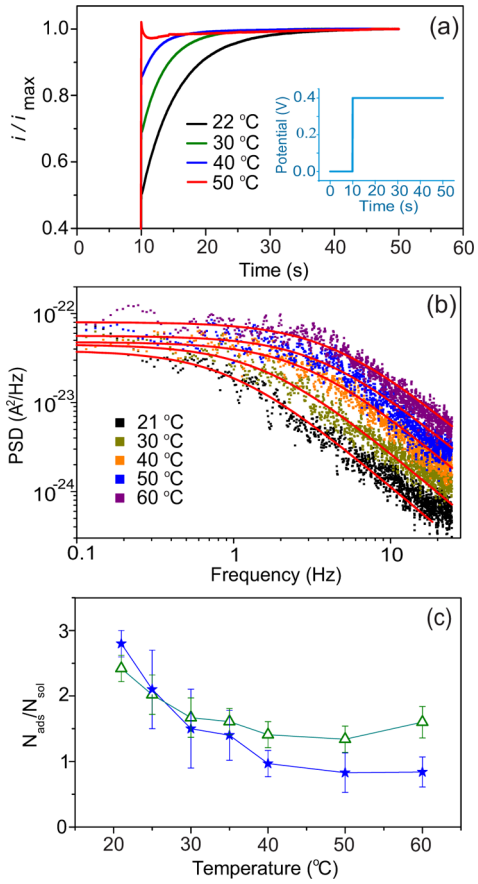

Figure 2. Redox-cycling measurements with 1 mM $Fc(MeOH)_2$ in 1 M KCl. (a) Transient response of the redox cycling current from a device of type 1 for a step change in the potential of the top electrode (inset) while the bottom electrode is held at 0 V. Each curve represents a different temperature, as indicated; the transient becomes shorter and less pronounced with increasing temperature, both trends reflecting a decrease in adsorption as discussed in the main text. (b) Power spectral density (PSD) of the fluctuations in the redox cycling current at different temperatures using a device of type 2. The shift of the PSD toward higher frequencies with increasing temperature reflects a combination of higher diffusion coefficients and decreasing adsorption. The red lines are fits from which values of the crossover frequency $f_{0,m}$ can be extracted. (c) Absolute degree of adsorption deduced from using eqs 1 (filled stars) and 2 (open triangles). The error bars represent the standard deviation from five consecutive measurements.

respectively, at 50 °C. These independent trends are mutually consistent.

Potential-step amperometry, while providing direct, qualitative evidence for adsorption, is sensitive only to differences in adsorption between two different electrode potentials. To measure the absolute amount of adsorbed molecules, we instead rely on electrochemical correlation spectroscopy, which probes fluctuations in the number of redox-active molecules inside the active volume resulting from Brownian motion. We have previously shown[19,23] that the random noise present in the redox cycling current is dominated by these intrinsic equilibrium fluctuations. The power spectral density (PSD) of the fluctuations, $S(f)$, takes the relatively simple form[19] $S(f) = S_{0,m}/(1 + (f/f_{0,m})^{3/2})$, where the crossover frequency $f_{0,m}$ is a parameter that quantifies the effect of Brownian motion. In the absence of adsorption, $f_{0,m}$ takes the ideal value $f_0 = (D/\pi)(3/(L_a^2(L_a + 6L_e)))^{2/3}$. Here L_a and L_e describe the channel geometry, as given in Figure 1a. In the presence of adsorption, the value of $f_{0,m}$ decreases below its ideal value; the absolute number of adsorbed molecules at both electrodes, N_{ads}, can then be extracted via the expression[19]

$$\frac{N_{ads}}{N_{sol}} = \frac{f_0}{f_{0,m}} - 1 \tag{1}$$

We measured the current–time fluctuations of the redox-cycling current under the same conditions as the data of Figure 2 a in type-2 devices with $L_e = 1$ μm and with the oxidizing and reducing electrodes set at 0.45 and 0 V, respectively; further details can be found in the SI. The corresponding PSDs are shown in Figure 2b. The spectra exhibit the expected form, crossing over from white noise at low frequencies to a $f^{-3/2}$ behavior above a characteristic frequency $f_{0,m}$. The crossover frequency clearly increases with increasing temperature, indicating that molecules can enter and exit the detection volume faster at higher temperatures. While one could expect an increase by a factor of 1.8 between 21 and 50 °C due to the increase in the diffusion coefficient D over this temperature range (SI), this is insufficient to explain the observed factor 4.3 change in $f_{0,m}$. We attribute the additional increase to a change in adsorption with temperature. Applying eq 1 yields the amount of adsorption, N_{ads}/N_{sol}, as a function of temperature, as shown by the filled stars in Figure 2 c. The adsorption decays monotonically with increasing temperature over the temperature range investigated, consistent with the qualitative conclusions from the transient measurements of Figure 2 a. Somewhat counterintuitively, N_{ads}/N_{sol} is found to be of order unity or higher. This is a direct consequence of the large surface-to-volume ratio: for a 1 mM solution in a 60 nm nanogap, $N_{ads}/N_{sol} = 1$ corresponds to a surface density of only 0.04 molecule per nm^2, well below full surface coverage.

In practice the spectral analysis described above requires extensive data and prior knowledge of the diffusion coefficient of the molecules. We have previously demonstrated that the degree of adsorption can also be extracted from the total amplitude of the redox-cycling current fluctuations, $I_{F,rms}$.[18] In short, this approach is model-independent and relies solely on the assumption that analyte molecules undergo independent Brownian motion. High adsorption translates into more molecules participating to the redox-cycling process, but each molecule contributes a smaller current; high adsorption thus leads to more averaging and smaller fluctuations, as indicated by the equation

$$\frac{N_{ads}}{N_{sol}} = \frac{1}{N_{sol}}\frac{I_F^2}{I_{F,rms}^2} - 1 \tag{2}$$

Here I_F is the average redox-cycling current and for most of the measurements described here $I_F = i_{lim}$. Strictly speaking, a correction is required to eq 2 to account for the transverse motion of redox molecules in and out of the active region because $w_t \neq w_b$, as shown in Figure 1b. Because these transverse fluctuations occur at relatively high frequencies and are thus masked by motion in the longitudinal direction, however, we simplify our analysis by neglecting these corrections. (See the SI for further details.)

The value of $I_{F,rms}$ is readily obtained from amperometric current–time traces. Figure 2 c shows the deduced degree of adsorption obtained using eq 2 (open triangles) as a function of temperature. The data once again show that an increase in

dx.doi.org/10.1021/jz402592n | J. Phys. Chem. Lett. 2014, 5, 636–640

temperature by ~20 °C above room temperature decreases the degree of adsorption by a factor of 2 to 3. Both eqs 1 and 2 yield similar adsorption values;[18] we ascribe the small mismatch at high temperatures to the uncertainty in determining I_F caused by small fluctuations in the temperature.

The measurements above show four separate ways in which adsorption of redox species is made manifest in nanogap devices. All of these exhibit consistent trends with temperature. For the remainder of this work, we concentrate on the method of eq 2 as it is general, quantitative, and straightforward to apply to experimental data.

The data of Figure 2 indicate that perhaps counterintuitively the positively charged oxidized form of $Fc(MeOH)_2$ exhibits enhanced adsorption at positively biased electrodes. This suggests that the adsorption might be mediated by the negatively charged anions in the supporting electrolyte. To investigate this scenario, we quantified the adsorption of $Fc(MeOH)_2$ for different supporting electrolyte anionic species while keeping the cationic species as K^+. The results are plotted in Figure 3. We find that the degree of adsorption increases

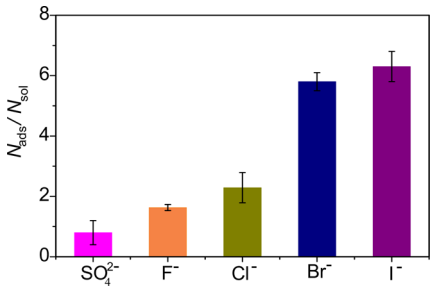

Figure 3. Degree of adsorption of $Fc(MeOH)_2$ versus anionic species present in the supporting electrolyte at room temperature. The degree of adsorption increases according to the sequence $SO_4^{2-} \sim F^- < Cl^- < Br^- < I^-$. The oxidizing and reducing electrodes were kept at 0.45 and 0 V, respectively.

according to the anion sequence $SO_4^{2-} \sim F^- < Cl^- < Br^- < I^-$. This sequence is closely related to the well-known Hofmeister series,[24,25] which was originally introduced to classify ions in terms of their ability to precipitate proteins. The relative effectiveness of anions or cations in a wide range of biochemical processes, for example, protein crystallization, colloidal systems, and the adsorption of cationic surfactants, to list a few, also follows the Hofmeister series.[26,27] The sequence SO_4^{2-}, F^-, Cl^-, Br^-, I^- also corresponds to the direction of decreasing free energy of hydration.[28] It is possible that anions, especially the ions such as Br^- and I^- with low hydration energy, can partially deform their hydration shell in favor of specific adsorption at the interface.[5] In support of this scenario, the observed sequence is close to the direction of increasing degree of specific adsorption of anions on metal electrodes given as F^-, SO_4^{2-}, Cl^-, Br^-, I^-.[4−6]

Details of the interactions of molecules at the electrode−electrolyte interface can be very complex. For example, many experimental studies in the literature point to the possibility of binding between the adsorbed anions and the oxidized molecules (ferrocenium ions). Surface ferrocenium ions can have entropically enhanced binding with low hydration energy anions present in the supporting electrolyte through ion pairing.[29−31] The formation energy of the ion pairs roughly scales with the solvation energies of the anions,[29] which is consistent with the Hofmeister series.

Surprisingly, we also observed a link between the type of anion and the limiting current: with nonadsorbing anions like F^- and SO_4^{2-}, we have observed decreased limiting currents and voltammograms representing slow reaction kinetics (see also SI). Similar observations were reported in measurements at nanoelectrodes with different supporting electrolytes.[32,33] These observations were ascribed to a range of different mechanisms including adsorption,[32] Frumkin and dynamic diffuse-layer effects,[33] and ion pairing.[34]

The molecule−electrode interactions driving adsorption can, of course, be species-dependent. We quantified the degree of adsorption for five commonly employed redox species, as summarized in Figure 4, all of which exhibited some degree of

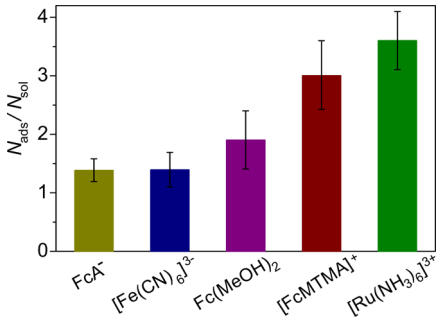

Figure 4. Degree of adsorption for five different redox molecules, ferrocene carboxylic acid (FcA^-), hexacyanoferrate-III ($[Fe(CN)_6]^{3-}$), 1,1 ferrocene dimethanol ($Fc(MeOH)_2$), (ferrocenyl methyl) trimethyl ammonium ($[FcMTMA]^+$), and hexaammine ruthenium ($[Ru(NH_3)_6]^{3+}$) at room temperature. The potentials at the oxidizing and the reducing electrode were 0.45 and 0 V, respectively (or 0 and −0.4 V for $[Ru(NH_3)_6]^{3+}$).

adsorption. Among these, FcA^- and $[Fe(CN)_6]^{3-}$ exhibited the lowest and $[Ru(NH_3)_6]^{3+}$ exhibited the highest degree of adsorption. This is in contradiction with the common assumption that $[Ru(NH_3)_6]^{3+}$ does not adsorb on noble metal (gold) electrodes in electrochemical quartz crystal microbalance studies.[12] Various other scenarios of the adsorption property of $[Ru(NH_3)_6]^{3+}$ were reported in the literature. For example, adsorption of positively charged $[Ru(NH_3)_6]^{3+}$ at negatively charged silica surfaces is used for preparing Ru-based catalysts.[17] Similarly, $[Ru(NH_3)_6]^{3+}$ adsorbs at anionic self-assembled monolayers (SAMs),[35] especially at the domain boundaries and defects formed on the SAM.[36] Singh et al.[18] also reported adsorption of $[Ru(NH_3)_6]^{3+}$ on bare platinum electrodes, where, contrary to other reports,[17,35,36] adsorption was found to decrease with increasing negative potentials on the electrodes. By analogy to the anion-mediated adsorption of $Fc(MeOH)_2$, we suggest that the counterintuitive adsorption behavior of $[Ru(NH_3)_6]^{3+}$ may be mediated by the excess cations near the electrodes at negative electrode potentials.

In summary, we have studied the adsorption of several outer-sphere electroactive species at Pt electrodes. We find that adsorption plays a significant role in both stepped-voltammetry and spectral measurements. Different degrees of adsorption were observed for several commonly employed outer-sphere redox couples, and surprisingly, $[Ru(NH_3)_6]^{3+}$, which is often considered as a particularly ideal species, exhibited the highest adsorption among the molecules we studied. Systematic investigations with $Fc(MeOH)_2$ suggest that its adsorption is mediated by the anionic species in the supporting electrolyte

dx.doi.org/10.1021/jz402592n | J. Phys. Chem. Lett. 2014, 5, 636−640

and follows the well-known Hofmeister series. Our results help to design measurement conditions where adsorption can be controlled, for example, in single-molecule electrochemistry measurements where excess adsorption mainly limits the signal-to-noise ratio.[21,22]

■ ASSOCIATED CONTENT

Supporting Information

Experimental procedures, detailed description about determination of adsorption, finite corrections, and cyclic voltammograms with supporting electrolytes of different anionic species. This material is available free of charge via the Internet at http://pubs.acs.org.

■ AUTHOR INFORMATION

Corresponding Author

*E-mail: s.g.lemay@utwente.nl. Phone: +31 53 489 2306. Fax: +31 53 489 3511.

Notes

The authors declare no competing financial interest.

■ ACKNOWLEDGMENTS

We gratefully acknowledge financial support from The Netherlands Organization for Scientific Research (NWO), the European Research Council (ERC), and the Semiconductor Research Corporation (SRC).

■ REFERENCES

(1) Bard, A. J.; Faulkner, L. R. *Electrochemical Methods Fundamentals and Applications*, 2nd ed.; John Wiley & Sons: , 2001.
(2) Finklea, H. O. Electrochemistry of Organized Monolayers of Thiols and Related Molecules on Electrodes. *Electroanal. Chem.* **1996**, *19*, 109−335.
(3) Pletcher, D.; Mitchell, P. J.; Hampson, N. A.; McNell, A. J. S. Adsorption at Solid Electrodes. In *Electrochemistry*; Royal Society of Chemistry: London, 1985; Vol. *10*, pp 1−84.
(4) Paik, W.-K.; Genshaw, M. A.; Kris, J. O. Adsorption of Anions at the Solid-Solution Interface. Ellipsometric Study. *J. Phys. Chem.* **1970**, *74*, 4266−4275.
(5) Magnussen, O. M. Ordered Anion Adlayers on Metal Electrode Surfaces. *Chem. Rev.* **2002**, *102*, 679−725.
(6) Tripkovic, D. V.; Strmcnik, D.; van der Vliet, D.; Stamenkovic, V.; Markovic, N. M. The Role of Anions in Surface Electrochemistry. *Faraday Discuss.* **2008**, *140*, 25−40.
(7) Grahame, D. C. The Electric Double Later and the Theory of Electrocapilarity. *Chem. Rev.* **1947**, *41*, 441−501.
(8) Timmer, B.; Rehbach, M. S.; Sluyters, J. H. Electrode Kinetics and Double Layer Structure. *Surf. Sci.* **1969**, *18*, 44−61.
(9) Lyklema, J. Points of Zero Charge in the Presence of Specific Adsorption. *J. Colloid Interface Sci.* **1984**, *99*, 109−117.
(10) Conway, B. E. Individual Solvated Ion Properties and Specificity of Ion Adsorption Effects in Processes at Electrodes. *Chem. Soc. Rev.* **1992**, *21*, 253−261.
(11) Frumkin, A. N.; Nikolajeva, N. V. On the Electroreduction of Anions. *J. Chem. Phys.* **1957**, *26*, 1552−1553.
(12) Lee, W. W.; White, H. S.; Ward, M. D. Depletion Layer Effects on the Response of the Electrochemical Quartz Crystal Microbalance. *Anal. Chem.* **1993**, *65*, 3232−3237.
(13) Stiles, R. L.; Balasubramanian, R.; Feldberg, S. W.; Murray, R. W. Anion-Induced Adsorption of Ferrocenated Nanoparticles. *J. Am. Chem. Soc.* **2008**, *130*, 1856−1865.
(14) Oja, S. M.; Wood, M.; Zhang, B. Nanoscale Electrochemistry. *Anal. Chem.* **2013**, *85*, 473−486.
(15) Ronkainen, N. J.; Halsall, H. B.; Heineman, W. R. Electrochemical Biosensors. *Chem. Soc. Rev.* **2010**, *39*, 1747−1763.
(16) Bocquet, L.; Charlaix, E. Nanofluidics, from Bulk to Interfaces. *Chem. Soc. Rev.* **2010**, *39*, 1073−1095.
(17) Jiao, L.; Regalbuto, J. R. The Synthesis of Highly Dispersed Noble and Base Metals on Silica via Strong Electrostatic Adsorption: I. Amorphous Silica. *J. Catal.* **2008**, *260*, 329−341.
(18) Singh, P. S.; Chan, H.-S. M.; Kang, S.; Lemay, S. G. Stochastic Amperometric Fluctuations as a Probe for Dynamic Adsorption in Nanofluidic Electrochemical Systems. *J. Am. Chem. Soc.* **2011**, *133*, 18289−18295.
(19) Zevenbergen, M. A. G.; Singh, P. S.; Goluch, E. D.; Wolfrum, B. L.; Lemay, S. G. Electrochemical Correlation Spectroscopy in Nanofluidic Cavities. *Anal. Chem.* **2009**, *81*, 8203−8212.
(20) Kang, S.; Mathwig, K.; Lemay, S. G. Response Time of Nanofluidic Electrochemical Sensors. *Lab Chip* **2012**, *12*, 1262−1267.
(21) Zevenbergen, M. A. G.; Goluch, E. D.; Singh, P. S.; Wolfrum, B. L.; Lemay, S. G. Stochastic Sensing of Single Molecules in a Nanofluidic Electrochemical Device. *Nano Lett.* **2011**, *11*, 2881−2886.
(22) Kang, S.; Nieuwenhuis, A. F.; Mathwig, K.; Mampallil, D.; Lemay, S. G. Electrochemical Single-Molecule Detection in Aqueous Solution using Self-Aligned Nanogap Transducers. *ACS Nano* **2013**, *7*, 10931−10937.
(23) Zevenbergen, M. A. G.; Krapf, D.; Zuiddam, M. R.; Lemay, S. G. Mesoscopic Concentration Fluctuations in a Fluidic Nanocavity Detected by Redox Cycling. *Nano Lett.* **2007**, *7*, 384−388.
(24) Kunz, W.; Henle, J.; Ninham, B. W. About the Science of the Effect of Salts. *Curr. Opin. Colloid Interface Sci.* **2004**, *9*, 19−37.
(25) Kunz, W.; Lo Nostro, P.; Ninham, B. W. The Present State of Affairs with Hofmeister Effects. *Curr. Opin. Colloid Interface Sci.* **2004**, *9*, 1−18.
(26) Para, G.; Jarek, E.; Warszynski, P. The Hofmeister Series Effect in Adsorption of Cationic Surfactants: Theoretical Description and Experimental Results. *Adv. Colloid Interface Sci.* **2006**, *122*, 39−55.
(27) Zhang, Y.; Cremer, P. S. Interactions between Macromolecules and Ions: The Hofmeister Series. *Curr. Opin. Chem. Biol.* **2006**, *10*, 658−663.
(28) Marcus, Y. Thermodynamic Functions of Transfer of Single Ions from Water to Non-Aqueous. *Pure Appl. Chem.* **1982**, *54*, 2327−2334.
(29) Rowe, G. K.; Creager, S. E. Redox and Ion-Pairing Thermodynamics in Self-Assembled Monolayers. *Langmuir* **1991**, *7*, 2307−2312.
(30) Acevedo, D.; Abruna, H. D. Electron-Transfer Study and Solvent Effects on the Formal Potential of a Redox-Active Self-Assembling Monolayer. *J. Phys. Chem.* **1991**, *95*, 9590−9594.
(31) Valincius, G.; Niaura, G.; Kazakevičienė, B.; Talaikytė, Z.; Kažemėkaitė, M.; Butkus, E.; Razumas, V. Anion Effect on Mediated Electron Transfer through Ferrocene-Terminated Self-Assembled Monolayers. *Langmuir* **2004**, *20*, 6631−6638.
(32) Beriet, C.; Pletcher, D. A Microelectrode Study of the Mechanism and Kinetics of the Ferro/Ferricyanide Couple in Aqueous Media: The Influence of the Electrolyte and its Concentration. *J. Electroanal. Chem.* **1993**, *361*, 93−101.
(33) Chen, S.; Kucernak, A. The Voltammetric Response of Nanometer-sized Carbon Electrodes. *J. Phys. Chem. B* **2002**, *106*, 9396−9404.
(34) Watkins, J. J.; White, H. S. Ion-Pairing Kinetics Investigated using Nanometer-size Pt Electrodes. *J. Electroanal. Chem.* **2005**, *582*, 57−63.
(35) Steichen, M.; Doneux, T.; Buess-Herman, C. On the Adsorption of Hexaammineruthenium (III) at Anionic Self-Assembled Monolayers. *Electrochim. Acta* **2008**, *53*, 6202−6208.
(36) Grubb, M.; Wackerbarth, H.; Wengel, J.; Ulstrup, J. Direct Imaging of Hexaamine-Ruthenium(III) in Domain Boundaries in Monolayers of Single-Stranded DNA. *Langmuir* **2007**, *23*, 1410−1413.

Supplementary information for

Reversible Adsorption of Outer-Sphere Redox Molecules at Pt Electrodes

Dileep Mampallil, Klaus Mathwig, Shuo Kang, Serge G. Lemay

MESA+ Institute for Nanotechnology, University of Twente, PO Box 217, 7500 AE Enschede, The Netherlands
Email: s.g.lemay@utwente.nl
Phone: +31 53 489 2306 Fax: +31 53 489 3511

S.1 Experimental methods

Potassium fluoride, potassium chloride, potassium bromide, potassium iodide, potassium sulfate, ferrocene carboxylic acid (FcCOOH), potassium hexacyanoferrate-III ($K_3Fe(CN)_6$), 1,1 ferrocene dimethanol ($Fc(MeOH)_2$), (ferrocenyl methyl) trimethyl ammonium iodide (FcMTMAI) and hexaammine ruthenium chloride ($Ru(NH_3)_6Cl_3$) were obtained from Sigma-Aldrich in analytical grade and used without further purification. Aqueous solutions of 1 mM $Fc(MeOH)_2$ were prepared with the above-mentioned salts as supporting electrolyte with concentration 1 M except for $K_2SO_4^{2-}$, whose concentration was only 0.68 M due to its limited solubility in water. Additionally, 1 mM solutions of all the above mentioned redox species were prepared in 1 M KCl as supporting electrolyte, except for FcCOOH whose supporting electrolyte was 200 mM PBS buffer with pH 6.5 due to solubility issues. Water was obtained from a Milli-Q Advantage ultrapure water system.

Nanogap devices were fabricated using lithographic techniques on a silicon substrate employing an approach reported previously [1, 2] except that photolithography was employed instead of electron-beam lithography. The fabricated devices contained two Pt electrodes separated by a Cr sacrificial layer. The active region of the device was defined as the volume encompassed by the overlapping top and bottom electrodes. We used two types of devices, Type 1 and Type 2, with $L_a \times w_b \times h = 100\,\mu\text{m} \times 3\ \mu\text{m} \times 130$ nm and $10\,\mu\text{m} \times 3\ \mu\text{m} \times 60$ nm, respectively. Type 1 devices were used for the transient measurements

in which the potential of one of the electrodes was stepped and the corresponding current transient was monitored (Fig. 2a in the main text). All other measurements were performed in Type 2 devices. There were two access holes located at the top of the devices. The distance between the edge of the top electrode and the access hole was L_e= 2 μm except for devices used for temperature varied measurements where L_e was 1 μm. Since the top electrode was wider than the bottom electrode, there are two inactive regions of width 1 μm, symmetrically located at both sides of the active region. In all the devices, directly before the measurements, the sacrificial layer was chemically removed using a wet chromium etchant (Selectipur) from BASF, at room temperature, thus forming the nanochannel. The etching procedure was monitored electrically by measuring the resistance between the top and the bottom electrodes.
Electrochemical experiments in the nanogap devices were performed with two Keithley 6430 subfemtoamp source meters used both as voltage sources to bias the electrodes and as current meters. The Keithley instruments were controlled remotely using Labview code. All potentials were applied at the electrodes with respect a 3 M Ag/AgCl reference electrode (BASi). No auxiliary electrode was used since the current through the reference electrode was appropriately small (in the range of pA, which is three orders of magnitude smaller than the redox-cycling current).

In the redox cycling measurements the potential at the reducing electrode was 0 V (or -0.4 V for $[Ru(NH_3)_6]^{3+}$) while that at the oxidizing electrode was swept between 0 V and 0.6 V. Current-time traces, each of length 50 s, were recorded at different temperatures ranging from room temperature (21 ± 2 °C) to 60°C by heating the metal slab over which the nanogap sensor was placed using a resistive element. The temperature was measured using a Pt-100 temperature sensor. From the steady state currents ($i = 4ner_0DN_B$, where N_B is the bulk number concentration of the redox species) measured using a glassy carbon ultra-microelectrode (UME) of radius, $r_0 = 5.5\,\mu$m (BASi MF-2007) the bulk diffusion coefficient D of $Fc(MeOH)_2$ molecules in 1 M KCl was determined at different temperatures.

S.2 Cleaning the electrodes

Prior to the redox cycling measurements, the devices were cleaned by filling with a solution of 0.5 M H_2SO_4 and repeatedly (typically 2 to 3 times) sweeping the electrode potential between -0.2 V and 1.2 V vs. Ag/AgCl until a reproducible voltammogram was obtained. A typical cyclic voltammogram obtained in this way from a nanogap device is shown in Fig. S1. The peaks (1) to (4) are representative for Pt in contact with H_2SO_4 [3]. This shows that a clean Pt surface is exposed to the solution.

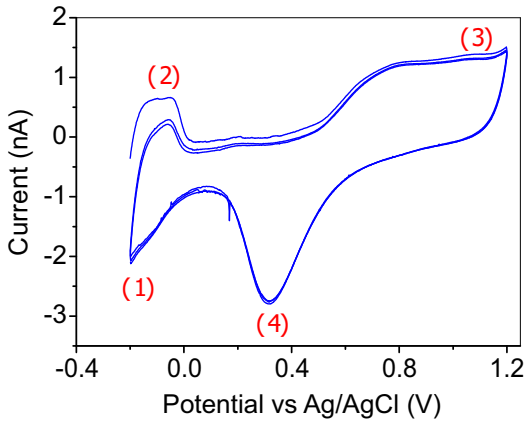

Figure S1: Cyclic voltammogram of a platinum electrode in a nanogap sensor filled with 0.5 M of H_2SO_4. The peaks correspond to: (1) hydrogen adsorption, (2) oxidation of the adsorbed hydrogen, (3) oxidation of platinum, (4) reduction of the platinum oxide layer. The scan rate is 50 mV/s.

S.3 Quantifying adsorption

To quantify adsorption using Eq. 2 in the main text one must determine the rms value of the fluctuations in the faradaic current, $I_{F,rms}$. As plotted in Fig. S2, we determined the degree of adsorption from the values of $I_{F,rms}$ obtained directly from the current-time traces (open squares) or from the PSD of the traces (open circles) as [4]

$$I_{F,rms} = \sqrt{\int S(f)df}. \tag{S1}$$

The integration is performed between the minimum (20 mHz) and the maximum (25 Hz) frequencies of the measured PSDs.

As the temperature increases, the frequency spectrum shifts towards higher values and frequency fluctuations beyond 25 Hz are not captured due to the limited data acquisition rate of the instrument. Therefore, the values of $I_{F,rms}$ determined in this way from the current-time traces at high temperature are not fully accurate. This is the reason why the initial decreasing trend in the adsorption in Fig. S2 (open circles and squares) disappears and above 35^{o}C the adsorption appears to increase as the temperature rises. To overcome this issue, we integrated the expression for the PSD ($S(f) = S_{0,m}/(1 + (f/f_{0,m})^{3/2})$) from $f = 0$ to $+\infty$ to include contributions from all frequencies. This results in the expression,

$$I_{F,rms} = \sqrt{2S_{0,m}\, f_{0,m}}. \tag{S2}$$

This means that if the values of S_0 and $f_{0,m}$ are obtained from fitting the PSD, it is then possible to get the correct value of $I_{F,rms}$ using Eq. S2. In Fig. S2, the degree of adsorption obtained using Eq. S2 is plotted (open triangles). These values are very close to the ones

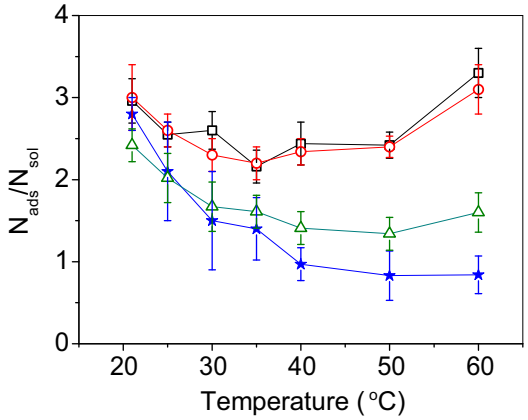

Figure S2: Degree of adsorption versus temperature obtained from the rms noise analysis using Eq. 2 (open symbols) and frequency analysis using Eq. 1 (filled symbols) for 1 mM $Fc(MeOH)_2$ in 1M KCl. In Eq. 2, the rms value of the fluctuations in the faradaic current can be obtained directly (black open squares) from the current-time traces or by integrating the PSD (red open circles) of the traces. As the temperature increases the frequency spectrum of the fluctuations goes beyond the detection bandwidth of the measurement device which brings inaccurate values of I_{rms} and adsorption. Integrating the PSD with frequencies ranging from 0 to ∞, however, gives correct values of I_{rms} and adsorption (green open triangles).

calculated using the frequency analysis (filled stars), as embodied by Eq. 1 in the main text, both showing a decreasing adsorption with increasing temperature.

Fig. S2 indicates that determining adsorption using $I_{F,rms}$ obtained directly from the current-time traces does not give correct values if a significant portion of the spectra is not included due to instrumental averaging. This becomes significant as $f_{0,m}$ approaches the measurement bandwidth at higher temperatures. However, at room temperature and when adsorption is large, this procedure is accurate and generates adsorption values similar to the ones obtained using Eq. 1 [5]. In all the measurements at room temperature (with devices having L_e= 2 μm) we determined the degree of adsorption using Eq. 2, with $I_{F,rms}$ directly obtained from the current-time traces.

S.4 Effect of the inactive region

The devices have two inactive region each of width 1 μm, symmetrically placed at each side of the active region due to the fact that the top electrode is broader than the bottom one. No redox cycling takes place in the inactive region as there is only one electrode (top) present. The transverse diffusion of molecules between the active and inactive regions causes high frequency fluctuations in the redox-cycling current. A detailed analytical derivation of the expressions to calculate the maximum power S_0 and cross-over frequency f_0 of these transverse and longitudinal fluctuations can be found in ref. [2]. These values

depend on the device geometry through the parameters L_e and L_a as,

$$S_0 = \frac{N i_p^2}{3D}(L_a^2 + 6L_e L_a) \tag{S3}$$

and

$$f_0 = \frac{D}{\pi}\left(\frac{3}{L_a^2(L_a + 6L_e)}\right)^{2/3}, \tag{S4}$$

where N is the average number of molecules present in the active region, D is the diffusion coefficient, and i_p is the current per molecule [2]. In the transverse case, taking $L_e = 1$ μm (width of the inactive region) and $L_a = 3$ μm (in this case, the width of the bottom electrode) we obtain S_0 is at least 100 times smaller than that of the longitudinal fluctuations taking $L_e = 1$ μm (the length of the access channel) and $L_a = 10$ μm (the length of the active region). Similarly, the cross-over frequency f_0 is 36 times larger than that of the longitudinal fluctuations. Therefore, since the longitudinal fluctuations mask the transverse fluctuations, to simplify our analysis we neglected any correction due to the inactive regions.

S.5 Temperature and limiting current

The diffusion-limited current in redox cycling is given by

$$I_F = \frac{neADcN_A}{h}, \tag{S5}$$

where n is the number of electrons transferred, $-e$ is the electron charge, A is the active area, N_A is the Avagadro constant, c is the molar concentration of the molecules and h is the distance between the top and bottom electrodes. Increasing the temperature also increases the diffusion-limited faradaic current, as shown in Fig. S3, because the value of the diffusion coefficient increases with temperature.

S.6 Cyclic voltammogram of $Fc(MeOH)_2$ and anions

We measured the redox-cycling current of $Fc(MeOH)_2$ while scanning the potential at the oxidizing electrode between 0 and 0.45 V. The experiments were performed with different anionic species in the supporting electrolyte and K^+ as cation. The results are shown in Fig. S4. With anions, F^- and SO_4^{2-}, the limiting current was considerably lower than the expected diffusion-limited value, obtained with Cl^-. The voltammogram for SO_4^{2-} further exhibits slow reaction kinetics. The half-wave potential (0.25 V) also changes for different anions.

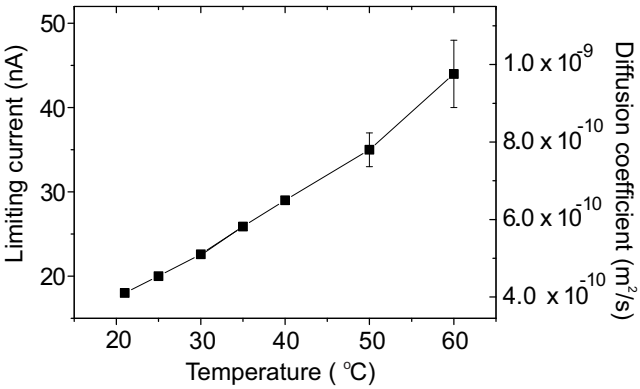

Figure S3: The diffusion limited steady state current for 1 mM $Fc(MeOH)_2$ in 1M KCl. The steady state current is directly proportional to the diffusion coefficient and increases with increasing temperature. The error bars are the standard deviations from five consecutive measurements.

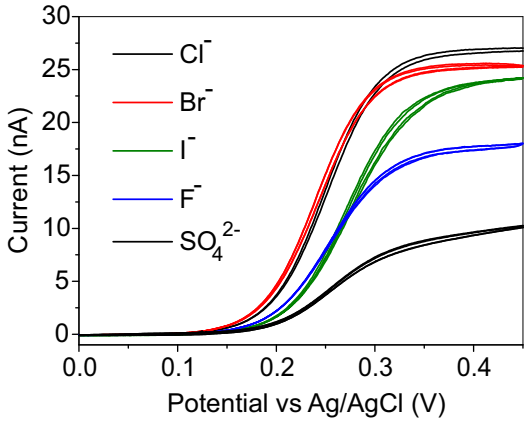

Figure S4: Cyclic voltammogram of 1 mM, $Fc(MeOH)_2$ with 1 M concentration of supporting electrolyte with different anions (shown in the figure). With SO_4^{2-} the reaction kinetics are found to be significantly slowed.

References

[1] Zevenbergen M. A. G.; Krapf D.; Zuiddam M. R. ; Lemay S. G. Mesoscopic Concentration Fluctuations in a Fluidic Nanocavity Detected by Redox Cycling, *Nano Lett.* **2007**, *7*, 384-388.

[2] Zevenbergen M. A. G.; Singh P. S.; Goluch E. D.; Wolfrum B. L.; Lemay S. G. Electrochemical Correlation Spectroscopy in Nanofluidic Cavities, *Anal. Chem.* **2009**, *81*, 8203-8212.

[3] Bard A. J.; Faulkner L. R. *Electrochemical Methods Fundamentals and Applications, 2nd Ed.*, John Wiley & Sons: New York; 2001.

[4] Stremler F. G. *Introduction to Communication Systems, 3rd Ed.*, Addison-Wesley Publishing Company: New York; 1990.

[5] Singh P.S.; Chan H.-S. M.; Kang S.; Lemay S. G. Stochastic Amperometric Fluctuations as a Probe for Dynamic Adsorption in Nanofluidic Electrochemical Systems, *J. Am. Chem. Soc.* **2011**, *133*, 18289 -18295.